

Vegetation-mediated surface soil organic carbon formation and potential carbon loss risks in Dongting Lake floodplain, China

Liyan Wang^{1, 2, 3}, Zhengmiao Deng^{1, 2}, Yonghong Xie^{1, 2}, Tao Wang^{1, 2}, Feng Li^{1, 2}, Ye'ai Zou^{1, 2},
Buqing Wang⁴, Zhitao Huo⁴, Cicheng Zhang⁵, Changhui Peng⁶, Andrew Macrae⁷

¹ Institute of Subtropical Agriculture, Chinese Academy of Sciences, Changsha 410125, China

² National Field Scientific Observation and Research Station of Dongting Lake Wetland Ecosystem in Hunan Province, Changsha 410125, China

³ University of Chinese Academy of Sciences, Beijing 100049, China

⁴ Changsha General Survey of Natural Resources Center, China Geological Survey, Changsha 410600, China

⁵College of Geographic Science, Hunan Normal University, Changsha 410081, China

⁶*Department of Biological Sciences, the University of Québec at Montreal, Montreal, QC H3C 3P8, Canada*

⁷Centro de Ciências da Saúde (CCS), Universidade Federal do Rio de Janeiro, BR 21941902, Brazil

Corresponding author: Zhengmiao Deng (dengzhengmiao@163.com) and Yonghong Xie (yonghongxie@163.com)

Abstract

Sources and stabilization mechanisms of soil organic carbon (SOC) fundamentally govern the carbon sequestration potential of wetland ecosystems. Nevertheless, systematic investigations regarding SOC sources and molecular stability remain scarce in floodplain wetland environments. This study employed dual analytical approaches (stable isotope analysis and ^{13}C nuclear magnetic resonance spectroscopy) to characterize surface SOC composition (0-20 cm) across three dominant vegetation communities (*Miscanthus*, *Carex*, and mudflat) in Dongting Lake floodplain wetlands. Key findings revealed: (1) Significantly elevated SOC concentrations in vegetated communities (*Miscanthus*: 13.76 g kg $^{-1}$; *Carex*: 12.98 g kg $^{-1}$) compared to unvegetated mudflat (6.88 g kg $^{-1}$); (2) Distinct $\delta^{13}\text{C}$ signatures across communities, with the highest isotopic values in *Miscanthus* (-22.67 ‰), intermediate in mudflat (-26.01 ‰), and most depleted values in *Carex* (-28.25 ‰); (3) Bayesian mixing models identified

32 autochthonous plant biomass as the primary SOC source (*Miscanthus*: $53.3 \pm 10.6\%$,
33 *Carex*: $52.4\% \pm 11.6\%$, mudflat: $47.5 \pm 12.5\%$); (4) Spatial heterogeneity in particulate
34 organic matter (POM) contributions across sub-lakes, showing descending
35 contributions from South (highest) > West > East (lowest) Dongting Lake; (5)
36 Molecular characterization revealed O-alkyl C dominance (30.5–46.8 %), followed by
37 alkyl C and aromatic C. Notably, *Miscanthus* soils exhibited enhanced O-alkyl C
38 content (44.75 %) (Alip/Arom:3.64) and reduced aromaticity (0.22) /hydrophobicity
39 (0.68) indices, suggesting comparatively lower biochemical stability of its SOC pool.
40 These results highlight the critical role of vegetation-mediated SOC formation
41 processes and warn against potential carbon loss risks in *Miscanthus*-dominated
42 floodplain ecosystems, providing a scientific basis for carbon management of wetland
43 soils.

44 **Keywords:** Floodplain wetland; Stable isotope; Soil carbon source; ^{13}C NMR; Organic
45 carbon stability

46 1 Introduction

47 Although wetlands occupy merely 5-8 % of the global terrestrial surface, they
48 disproportionately store 20-30 % of the terrestrial carbon, positioning them as pivotal
49 regulators in global carbon cycling (Kayranli et al., 2010; Köchy et al., 2015; Mitsch et
50 al., 2013). Small changes in wetland soil organic carbon (SOC) stocks may have large
51 feedback effects on climate-carbon cycle interactions. The long-term carbon
52 sequestration capacity of wetland ecosystems is jointly governed by two critical factors:
53 carbon input dynamics and biochemical stabilization mechanisms. Therefore, clarifying
54 the sources and stabilization pathways of wetland SOC is essential for optimizing
55 carbon sink management and enhancing climate change mitigation strategies.

56 In floodplain systems, the organic carbon in sediment derives from both
57 autochthonous (in-situ plant biomass and aquatic plankton) and allochthonous sources
58 (river-transported particulate organic matter, POM) (Robertson et al., 1999). The
59 sources of SOC vary significantly among different vegetation communities, depending
60 on vegetation characteristics and hydrological conditions (Ni et al., 2025; Guo et al.,

61 2025). For instance, in mangrove ecosystems, SOC is primarily derived from mangrove
62 plant tissues, whereas in adjacent *S. alterniflora* marshes and tidal flats, it relies more
63 heavily on fluvially imported particulate organic matter (POM) (Wang et al., 2024a).
64 Vegetation influences SOC sources mainly through plant productivity and litter
65 decomposition rates, while hydrological conditions regulate the input and deposition of
66 allochthonous carbon (Guo et al., 2025; Xia et al., 2021). Moreover, even within the
67 same type of vegetation community, SOC sources may exhibit spatial heterogeneity due
68 to local topographic features and anthropogenic activities, leading to the accumulation
69 of allochthonous carbon (Swinnen et al., 2020). Despite these insights, critical
70 knowledge gaps persist regarding interspecific differences in carbon sourcing among
71 co-occurring vegetation communities within floodplain wetlands and the spatial scaling
72 of these heterogeneities. Stable carbon and nitrogen isotopes have been widely used to
73 analyze the sources of wetland SOC (Sasmito et al., 2020; Wu et al., 2021a).

74 SOC stability is defined as the capacity of organic compounds to
75 resist changes and/or losses (Doetterl et al., 2016). Enhanced SOC stability typically
76 corresponds with preferential accumulation of recalcitrant compounds that withstand
77 microbial degradation. ^{13}C nuclear magnetic resonance (NMR) is widely used to
78 analyze the chemical composition of SOC, and can calculate the relative abundance of
79 various C functional groups closely related to SOC decomposition (Shen et al., 2018).
80 Biochemically recalcitrant components include alkyl-C and aromatic-C, whereas labile
81 components comprise O-alkyl-C and carbonyl-C (Skjemstad et al., 1994) .
82 Consequently, soils enriched in labile SOC fractions demonstrate heightened
83 vulnerability to carbon loss through accelerated decomposition pathways, particularly
84 under environmental disturbance. These molecular signatures are regulated by factors,
85 including vegetation inputs (via lignin/cellulose ratios and aliphatic content), soil
86 properties (clay-silt particle associations), and climatic controls on vegetation litter
87 decomposition (Cano et al., 2002; Chen et al., 2018; Liu et al., 2022; Preston et al.,
88 1994; Quideau et al., 2001; Wu et al., 2020). In floodplain environments, hydrologic
89 conditions further regulate SOC components by affecting oxygen supply and altering

90 microbial metabolism and enzyme activity (Kirk and Farrell, 1987; Boye et al., 2017).
91 However, there are insufficient studies on the sources and stability of SOC in floodplain
92 wetlands.

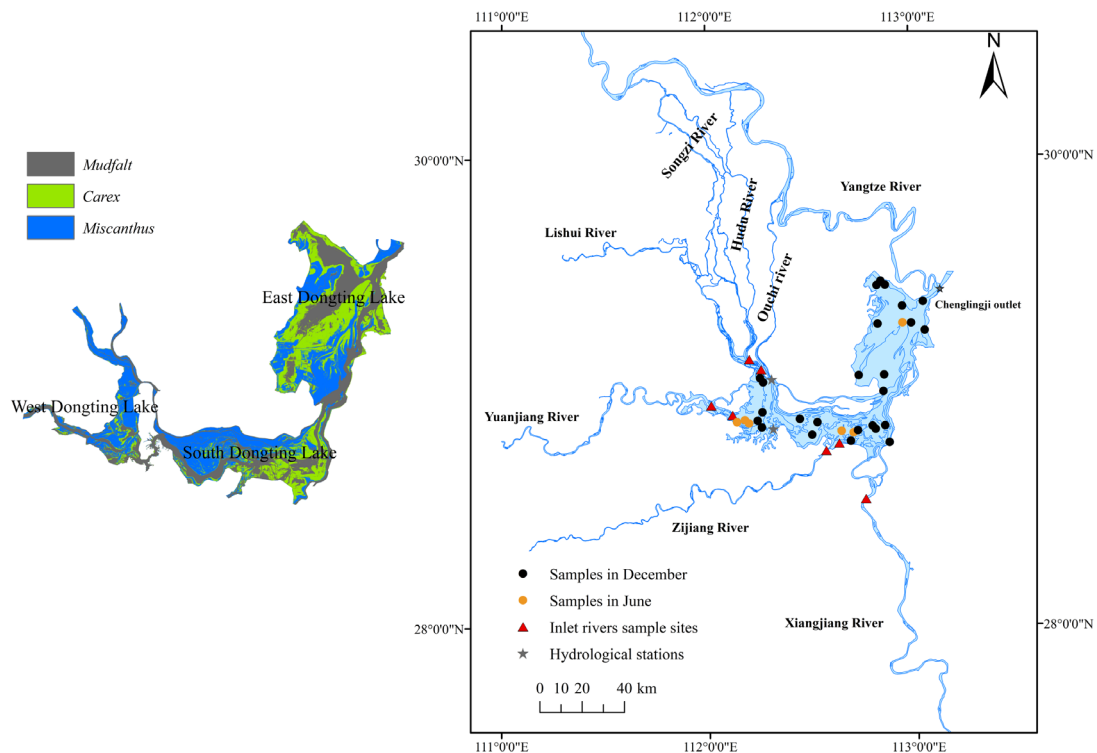
93 Dongting Lake, a Yangtze River-connected floodplain wetland, presents an ideal
94 natural laboratory for investigating these processes. Its elevation-dependent vegetation
95 zonation and complex topography create pronounced gradients in carbon source inputs
96 and stabilization conditions. Among soil carbon pools, surface SOC is more susceptible
97 to the effects of climate, hydrological conditions and human activities, resulting in a
98 high carbon turnover rate and requiring more attention. In this study, stable isotope
99 techniques were used to analyze the source of surface SOC and the stability of SOC
100 was further evaluated using the ^{13}C NMR method. The hypotheses of this study were
101 as follows: (1) Regarding vegetation communities, SOC content was expected to be
102 highest in the *Miscanthus* community, intermediate in the *Carex* community, and lowest
103 in the mudflat. This was based on the corresponding gradient in plant biomass input.
104 Spatially, a gradient of East > South > West Dongting Lake was anticipated, owing to
105 the longer inundation durations in East Dongting Lake, which promote anaerobic
106 conditions that suppress SOC decomposition. (2) SOC in the *Miscanthus* and *Carex*
107 communities would be primarily originate from autochthonous plant sources, driven by
108 in-situ plant litter deposition. In contrast, SOC in the mudflat would primarily originate
109 from allochthonous, derived from particulate organic matter delivered by hydrological
110 processes due to the lack of local vegetation. (3) Due to differences in SOC sources, the
111 SOC structure in the *Miscanthus* and *Carex* communities was hypothesized to be
112 dominated by O-alkyl C (reflecting plant-derived carbohydrates like cellulose).
113 Conversely, the SOC in the mudflat was expected to be richer in aromatic C, as
114 allochthonous organic matter often contains more recalcitrant components.

115 **2 Materials and methods**

116 **2.1 Study areas**

117 Dongting Lake ($28^{\circ}30'–30^{\circ}20'\text{N}$, $111^{\circ}40'–113^{\circ}10'\text{E}$) is the second largest inland
118 freshwater lake in China, with an area of 2564 km^2 . It comprises East Dongting Lake

119 (EDL, 1327.8 km²), West Dongting lake (WDL, 443.9 km²) and South Dongting Lake
 120 (SDL, 920 km²) (Gao et al., 2001). The Lake is a typical river-connected lake that
 121 mainly receives inflow from the Yangtze River through three channels (the Songzi,
 122 Hudu, and Ouchi Rivers) and other four tributaries (the Xiang, Zi, Yuan, and Li Rivers)
 123 and then outflows into the Yangtze River from the Chenglingji outlet (Deng et al., 2018).
 124 The lake's water level exhibits significant seasonal fluctuations, with flood periods
 125 occurring from June to October. From the water's edge to the uplands, the dominant
 126 vegetation communities include Mudflat communities, *Carex* spp. (Cyperaceae)
 127 communities, and *Miscanthus sacchariflorus* (Poaceae) communities (Xie et al.,
 128 2015). The study area is characterized by a humid subtropical monsoon climate with a
 129 mean annual temperature of 16.8°C and a mean annual precipitation of 1382 mm.



130
 131 **Figure 1.** Map of the study area and sampling sites.

132 **2.2 Field sampling and parameter measurement**

133 Soil sampling was conducted across three dominant vegetation during December
 134 2022, with supplementary Mudflat sediment sampling in June to account for

135 hydrological accessibility constraints. The final sampling comprised 31 sampling sites
136 (11 Mudflat, 8 *Carex* community, 12 *Miscanthus* community) with latitude and
137 longitude recorded using a hand-held global positioning system (GPS). Notably, *Carex*
138 communities in West Dongting Lake were excluded from sampling due to insufficient
139 population density. At each sampling site, a 1x1 m sample plot was set up, and surface
140 (0-20 cm, 500 g fresh soil) soil samples were collected from five points in the plot and
141 mixed for subsequent analysis. For vegetated sites (*Carex* and *Miscanthus*
142 communities), aboveground tissue, surface litter layer and belowground roots were
143 collected from the sample plots. All samples were transported to the laboratory. Soil
144 samples were air-dried in a cool, ventilated area and passed through a 2 mm sieve. The
145 sieved soil was split into two portions by quartering, with one portion being finely
146 ground to pass through a 0.147 mm sieve for subsequent analysis. Plant material was
147 dried at 60° C to a constant mass and the dry weight was recorded prior to pulverization.
148 Both SOC and plant organic carbon content was quantified using the potassium
149 dichromate-sulfuric acid oxidation technique. The TN content of soil was measured
150 using an elemental analyzer (Vario MAX CNS, Elementar, Germany). The formula for
151 calculating vegetation organic carbon stocks (VOCS) is as follows:

$$152 \quad VOCS = A \times VB \times VOC \quad (1)$$

153 Where A is the vegetation distribution area (km^2), VB is the vegetation biomass
154 (t/km^2), VOC is the vegetation organic carbon content ($t C / t$ biomass).

155 **2.3 Inundation duration and runoff volume**

156 We used the hydrological data from Chenglingji, Xiaohezui, and Nanzui
157 hydrological stations to calculate the inundation time and runoff volume of EDL, SDL,
158 and WDL, respectively. The hydrological data from Chenglingji, Xiaohezui and Nanzui
159 have been widely used to analyze the hydrological characteristics of EDL, SDL and
160 WDL. Vegetation is classified as submerged when water levels exceed specific
161 elevations. Using daily water levels and elevation data from the Dongting Lake Wetland
162 DEM (Geospatial Data Cloud: <http://www.gscloud.cn>), we calculated vegetation-
163 specific inundation durations. The inundation duration (ID) for each site was calculated

164 as the total number of days within a year when the daily water depth (WD) was greater
165 than zero. This was computed using a daily indicator function, summed over the entire
166 year:

167 $ID = \sum_{i=1}^n \mathbf{1}_{\{WD_i > 0\}}$ (2)

168 where n is the total number of days in a year, i is the day index, and $\mathbf{1}_{\{WD_i > 0\}}$ is
169 the indicator function which takes the value of 1 if the condition $WD_i > 0$ is true on the
170 i-th day, and 0 otherwise.

171 The daily water depth WD_i was computed as:

172 $WD_i = WL_i - E$ (3)

173 where WL_i is the daily water level (m) at the Chenglingji (EDL), Xiaohezui (SDL),
174 and Nanzui (WDL) Hydrological Stations, and E is the elevation (m).

175

176 2.4 Stable isotope analysis and mixing model

177 The soil samples (2 g) were added to 0.5 mol/L hydrochloric acid reflections for
178 24 h to removal carbonates, then washed to neutrality with distilled water and dried at
179 55 °C. The treated soil samples were ground through a 0.147 mm sieve and used for
180 stable isotope measurements. $\delta^{13}\text{C}$ and $\delta^{15}\text{N}$ stable isotope ratios were measured using
181 the Element Analyses-Isotope Ratio Mass Spectrometry (EA-IRMS) (Delta V
182 advantage, Thermo Fisher) and were calculated from the following equation:

183 $\delta(\text{‰}) = ((R_{sample}/R_{standard}) - 1) \times 1000$ (4)

184 where R_{sample} is the stable $^{13}\text{C}/^{12}\text{C}$ or $^{15}\text{N}/^{14}\text{N}$ isotope ratio of the sample, and $R_{standard}$ is
185 stable the $^{13}\text{C}/^{12}\text{C}$ or $^{15}\text{N}/^{14}\text{N}$ isotope ratios of the international isotope standard (Vienna
186 Peedee Belemnite and N₂ in the atmosphere, respectively).

187 SOC potential sources include *Miscanthus* plant, *Carex* plant and Plankton, and
188 rivers suspended particulate organic matter (POM). In addition to plankton, we
189 collected other potential end-members for stable isotope analysis. Five samples of
190 aboveground tissues, surface litter and root of *Miscanthus* and *Carex* plants were
191 randomly sampled. Due to the construction of the Three Gorges Dam, the POM entering
192 Dongting Lake changed from three channels (the Songzi, Hudu, and Ouchi Rivers) to

193 four tributaries (the Xiang, Zi, Yuan, and Li Rivers) (Wang et al., 2024b). Therefore,
194 we collected POM at the inlets of the Xiang, Zi, Yuan, and Li Rivers into the lake. The
195 POM from the Yuan and Li Rivers served as the allochthonous end-members for WDL,
196 while the POM from the Xiang, Zi, Yuan, and Li Rivers served as the allochthonous
197 end-members for EDL and SDL (Fig. 1).

198 Source contributions were quantified using a Bayesian mixing model based on
199 $\delta^{13}\text{C}$ and $\delta^{15}\text{N}$. The MixSIAR model combines the advantages of SIAR and MixSIR. It
200 not only introduces fixed and random effects, but also incorporates source uncertainty.
201 These features endow the MixSIAR model with higher source analysis accuracy, and it
202 has been widely used in wetland sediments (Zhang et al., 2024). In the Bayesian mixing
203 model, the Markov chain Monte Carlo (MCMC) algorithm was set to "normal". Model
204 convergence was assessed using Gelman-Rubin diagnostics and Geweke diagnostics
205 (Stock and Semmens, 2016). Additionally, an "uninformative" prior was selected, and
206 the error structure was defined as "residual and process error".

207 **2.5 ^{13}C NMR analysis and spectral indices**

208 The chemical structure of SOC was determined by solid-state ^{13}C NMR
209 spectroscopy. In order to improve the signal-to-noise ratio, soil samples are pretreated
210 with hydrofluoric acid (HF) before ^{13}C NMR spectroscopy analysis. Soil samples (8.0
211 g) were placed into 100 mL plastic centrifuge tubes containing 50 mL of 10% (v/v) HF
212 solution. The tubes were shaken on a shaking bed at 200 rpm for 1 hour at 25 °C, then
213 centrifuged at 3800 rpm for 5 minutes. After discarding the supernatant, the residual
214 soil was subjected to repeated HF treatments under identical conditions. The entire
215 procedure was conducted 8 times with the following shaking durations: 1 hour for the
216 first 4 cycles, 12 hours for cycles 5-7, and 24 hours for the final cycle. The treated
217 residue was washed 5-6 times with distilled water to remove the HF solution. The
218 residue was dried in an oven at 40 °C and sieved through 0.25 mm sieve. Subsequently,
219 pretreated samples were analyzed using a Bruker AVANCE III HD 600MHz
220 spectrometer equipped with an H/X dual-resonance solid probe, operating in CP/MAS
221 mode. Experimental parameters were set as follows: 4-mm ZrO_2 rotor spinning at 10

222 kHz, ^{13}C detection resonance frequency of 150 MHz, acquisition time of 6.25 μs , and
223 spectral width of 30 kHz.

224 The spectra of samples were divided in the following chemical shift regions: 0–45
225 ppm (alkyl C, originating from Microbial metabolites and plant biopolymers), 45–110
226 ppm (O-alkyl C, derived from carbohydrates), 110–160 ppm (aromatic C, derived from
227 lignin, polypeptides and black carbon) and 160–220 ppm (carbonyl C, derived from
228 fatty acids, amino acids and lipids). The relative abundances of different carbon
229 functional groups were quantitatively determined by integrating their respective peak
230 areas in the solid-state ^{13}C NMR spectra. Subsequent spectral analyses were performed
231 using MestReNova software (12.0.0-20080) for statistical interpretation of the data.
232 SOC spectra of the different communities are provided in the Appendix A (Fig. S1).
233 According to (Boeni et al., 2014; Wang et al., 2023), four indicators of the stability of
234 SOC were calculated as:

235 (1) A/O-A, which is used to indicate the degree of humification of SOC, the higher
236 the value, the more resistant it is to decomposition;

237 $\text{A/O-A} = \text{alkyl C} / \text{O-alkyl C}$ (5)

238 (2) Alip/Arom, which is used to indicate the complexity of the molecular structure
239 of humus, the higher the ratio, the simpler the molecular structure;

240 $\text{Alip/Arom} = (\text{alkyl C} + \text{O-alkyl C}) / \text{aromatic C}$ (6)

241 (3) aromaticity index (AI), which is used as measure of the complexity of SOC
242 structure;

243 $\text{AI} = \text{aromatic C} / (\text{alkyl C} + \text{O-alkyl C} + \text{aromatic C})$ (7)

244 (4) hydrophobicity index (HI), which is used to indicate the stability of SOC
245 integrated with aggregates.

246 $\text{HI} = (\text{alkyl C} + \text{aromatic C}) / (\text{O-alkyl C} + \text{carbony C})$ (8)

247 **2.6 Statistical analysis**

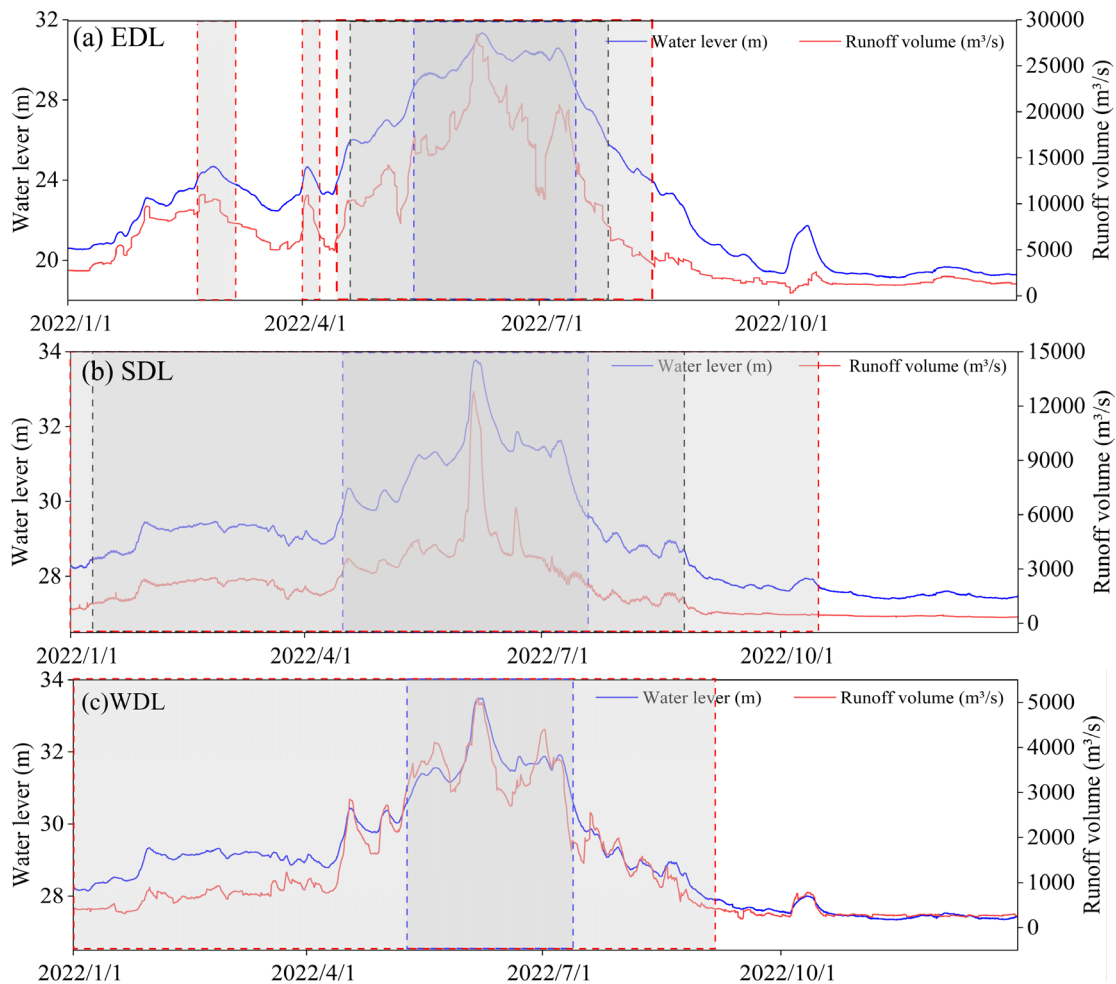
248 The Shapiro-Wilk test and the Levene test are used respectively to test the
249 regularity and consistency of the data. Differences between community were evaluated
250 through one-way analysis of variance (ANOVA); multiple comparisons were performed

251 using the least significant difference (LSD) test. Nonparametric tests were used for data
 252 that did not meet homogeneity of variance. A threshold of $P < 0.05$ was used to denote
 253 statistically significant differences. Source contributions were quantified using the
 254 “MixSIAR” package in R.

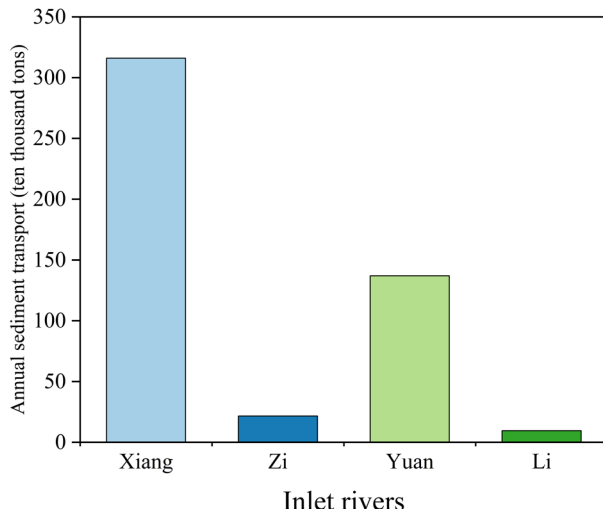
255

256 **3 Results**

257 **3.1 Hydrological Characteristics of East, South and West Dongting Lakes**



258 **Figure 2.** Water level, Runoff volume and inundation duration in EDL, SDL, and WDL.
 259 In the figure, the shaded part represents submerged, with the red, black, and blue dashed
 260 boxes respectively indicating the Mudflat, *Carex*, and *Miscanthus* communities. EDL:
 261 EDL: East Dongting Lake; SDL: South Dongting Lake; WDL: West Dongting Lake.



263

264 **Figure 3.** The annual sediment transport of inlet rivers in 2022.

265 The water level of Dongting Lake shows significant fluctuations (19.24-33.78 m)
 266 (Fig.2). There were differences in the inundation duration of different vegetation
 267 communities, with the Mudflat having the longest inundation duration (223.8 d),
 268 followed by *Carex* (162.4 d), and *Miscanthus* having the shortest inundation time (78.9
 269 d). Among the sub-lakes, SDL showed the longest inundation time (206.8 d), followed
 270 by WDL (152 d) and EDL (102.8 d). The annual runoff volume was the highest in EDL,
 271 followed by SDL and WDL. The annual sediment transport of four tributaries was 484.1
 272 $\times 10^4$ tons, with the Xiangjiang River having the highest annual sand transport (Fig.3).

273 **3.2 Carbon sink capacity in dominant vegetation community**

274 The area of Dongting Lake wetland spans 2564.1 km^2 , with vegetation distribution
 275 dominated by the *Miscanthus* community (36.9 %), followed by the Mudflat (33.0 %)
 276 and the *Carex* community (30.1 %) (Table 1). *Miscanthus* community exhibited
 277 significantly higher plant biomass (2922.9 t/km^2) and tissue carbon content (454.7 g kg^{-1}
 278 than *Carex* community (1391.0 t/km^2 and 422.4 g kg^{-1} , respectively; $P <$
 279 0.05). Consequently, its organic carbon stock ($1.258 \pm 0.13 \text{ Tg C}$) nearly tripled that
 280 of *Carex* communities, representing 72.5 % of the wetland's total vegetation-mediated
 281 carbon storage.

282 **Table 1.** Distribution area, biomass, organic carbon content and carbon stock in
 283 dominant vegetation community.

284

Community types	Areas(km ²)	vegetation biomass (t/km ²)	vegetation organic carbon content (g kg ⁻¹)	vegetation organic carbon storage (Tg C)
<i>Miscanthus</i>	946.74	2922.9±300.8a	454.7±6.22a	1.258±0.13a
<i>Carex</i>	770.63	1391.0±269.7b	422.4±4.75b	0.453±0.09b
<i>Mudflat</i>	846.72	0	0	0

285 The expressed data represents mean ± standard error.

286

287 **3.3 Stable isotope of soil and vegetation**

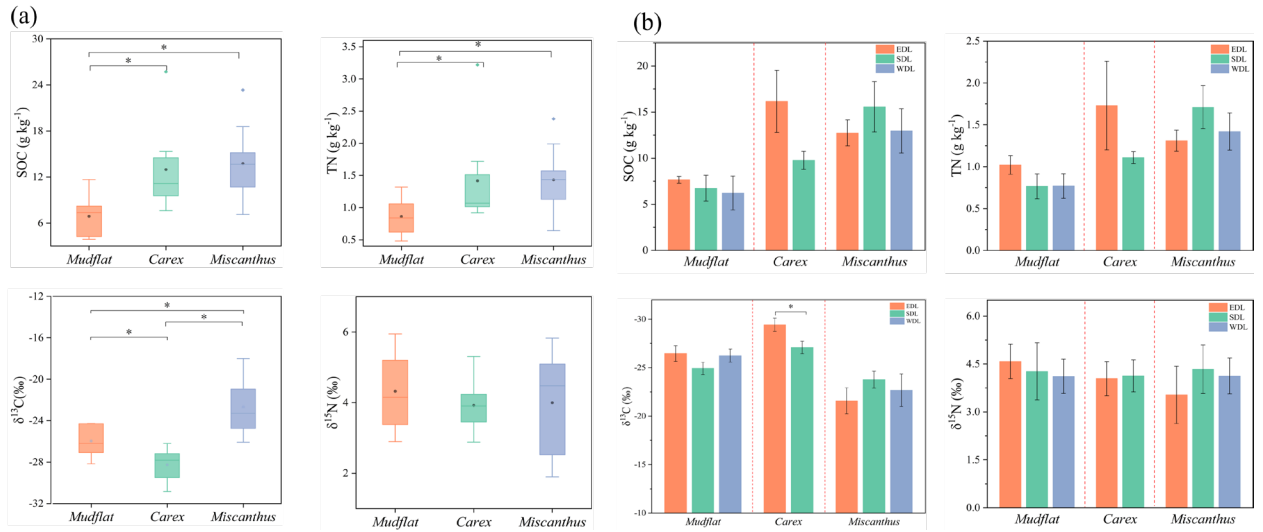
288 *Miscanthus* plants displayed the most enriched $\delta^{13}\text{C}$ values (-13.85 ‰ to -17.24 ‰), contrasting with plankton-derived carbon showing the most depleted signatures. Conversely, $\delta^{15}\text{N}$ values followed an inverse pattern, with plankton exhibiting the highest enrichment (Table 2). There were differences in SOC and TN contents among community types, with the *Miscanthus* and *Carex* communities having significantly higher SOC and TN contents than the Mudflat community ($P < 0.05$, Fig. 4a).

295 The soil $\delta^{13}\text{C}$ value ranged from -30.85 to -18.01‰ (-25.30±0.54 ‰) with the highest values were observed in *Miscanthus* (-18.01 to -26.08 ‰) ($P < 0.05$, Fig. 4a), followed by *Mudflat* (-24.3 to -28.68 ‰) and *Carex* (-27.08 to -30.85 ‰). There was no significant difference in soils $\delta^{15}\text{N}$ values from different vegetation types. EDL *Carex* communities were smaller in $\delta^{13}\text{C}$ compared to SDL ($P < 0.05$, Fig. 4b), while other vegetation types showed no significant inter-regional differences in SOC, TN, $\delta^{13}\text{C}$ or $\delta^{15}\text{N}$ across sub-basins (Fig. 4b).

302 **Table 2.** Carbon and nitrogen stable isotope signatures (‰) of different potential end-members

Sources	$\delta^{13}\text{C}$ (‰)	$\delta^{15}\text{N}$ (‰)	304
<i>Miscanthus</i> Plant	-14.46±0.63	0.2±1.45	305
<i>Carex</i> Plant	-29.51±0.27	2.42±1.03	306
EDL+SDL POM	-29.31±1.08	6.38±1.5	307
WDL POM	-29.22±1.40	6.08±1.82	308
Plankton*	-30.0 ±6.60	6.5±0.75	309

310 * C and N stable isotope signature of Plankton were cited from (Kendall et al., 2001;
311 Li et al., 2016)



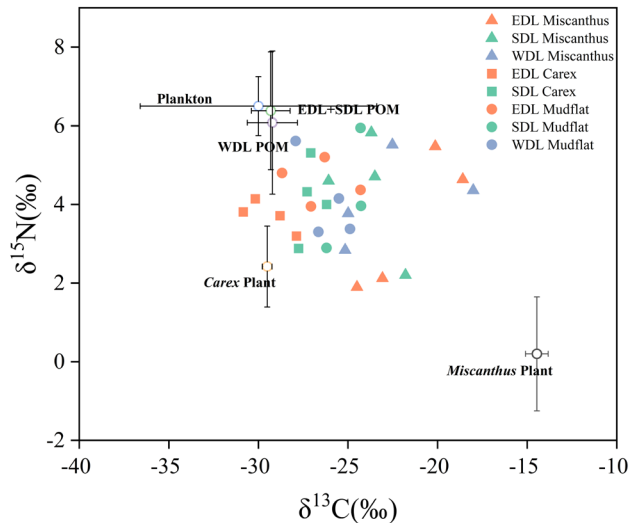
312

313 **Figure 4.** Characteristics of SOC, TN, $\delta^{13}\text{C}$ and $\delta^{15}\text{N}$ with vegetation types (a), and in
 314 different sub lakes(b). EDL: East Dongting Lake; SDL: South Dongting Lake; WDL:
 315 West Dongting Lake. * indicates significant differences between different vegetation
 316 types at the $P<0.05$ level.

317 **3.4 SOC sources and contribution**

318 The isotopic composition of all soil samples fell within the mixing space
 319 delineated by potential end-members, confirming their effectiveness in source
 320 discrimination (Fig. 5). Our study showed autochthonous plant (including *Miscanthus*
 321 and *Carex* plant) was the main source of SOC in Dongting floodplain wetland
 322 (*Miscanthus*: $53.3\pm10.6\%$, *Carex*: $52.4\pm11.6\%$, mudflat: $47.5\pm12.5\%$)(Fig. 6a).
 323 Allochthonous POM contributions exhibited significant variation across vegetation
 324 types, with minimum values in *Miscanthus* communities ($26.8\pm8.1\%$) versus *Carex*
 325 ($31.3\pm8.3\%$) and mudflat ($35.4\pm10.2\%$).

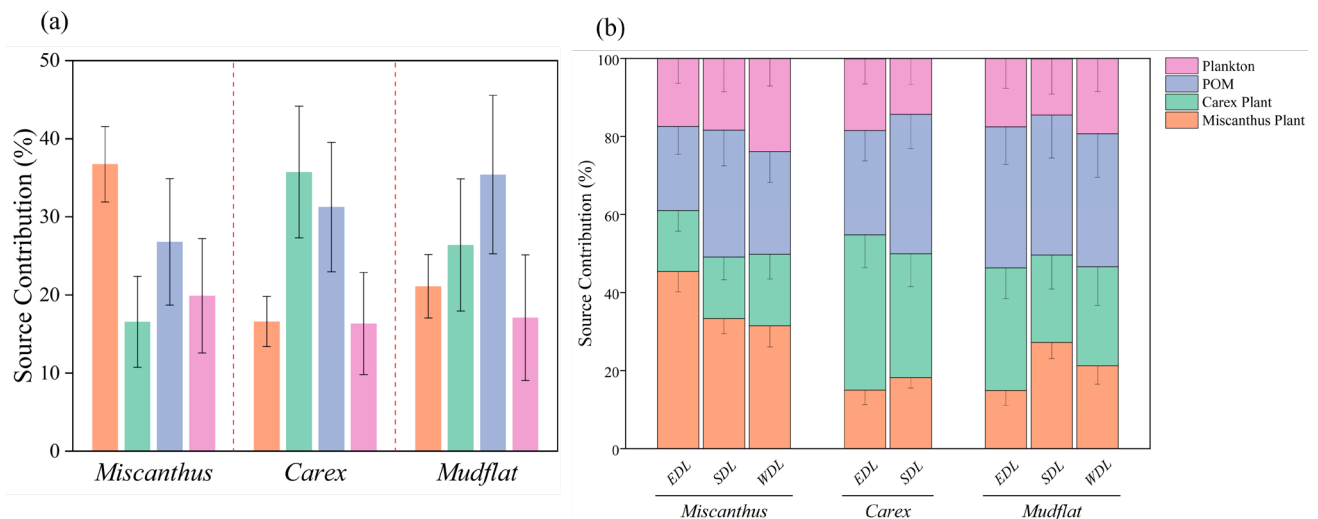
326 Spatial heterogeneity in carbon source contributions was evident across vegetation
 327 types (Fig. 6b). In *Miscanthus* communities, EDL demonstrated maximal
 328 autochthonous input dominance (12.1% and 13.9% greater than SDL and WDL
 329 respectively), whereas allochthonous POM displayed inverse spatial patterns (10.9%
 330 and 4.7% lower than SDL and WDL respectively). In *Carex* communities, EDL showed
 331 8.1% higher in autochthonous contributions relative to SDL, concomitant with 9.1%
 332 reduce in POM inputs compared to SDL.



333

334 **Figure 5.** The end-element plots of $\delta^{13}\text{C}$ and $\delta^{15}\text{N}$ values for samples of Dongting Lake
 335 soil and SOC sources. EDL: East Dongting Lake; SDL: South Dongting Lake; WDL:
 336 West Dongting Lake.

337



338

339 **Figure 6.** Relative contributions of SOC sources with vegetation types (a) and in
 340 different sub lakes (b). POM: particulate organic matter; EDL: East Dongting Lake;
 341 SDL: South Dongting Lake; WDL: West Dongting Lake.

342

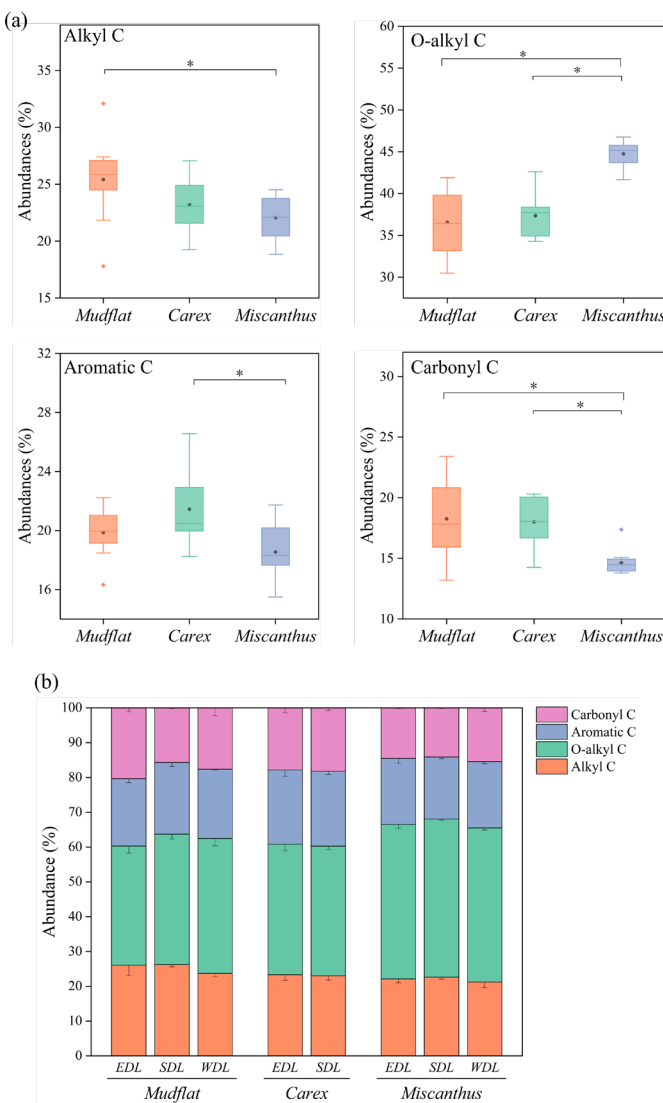
343 3.5 Chemical structure and SOC stability

344 SOC functional groups were dominated by O-alkyl C (30.5–46.8 %), followed by
 345 alkyl C (17.8–32.1 %) and aromatic C (15.5–26.6 %), with Carbonyl C exhibiting
 346 minimal abundance. The highest abundance of alkyl C was observed in mudflat

347 community ($25.4 \pm 1.2 \%$), followed by *Carex* ($23.2 \pm 0.9 \%$), and then *Miscanthus*
 348 community ($22.1 \pm 0.6 \%$) ($P < 0.05$, Fig. 7a); O-alkyl C shows the opposite trend. The
 349 abundances of aromatic C were significantly higher in the *Carex* community than
 350 *Miscanthus* (Fig. 7a, $P < 0.05$). Carbonyl C showed the same trend as alkyl C. There
 351 were no significant changes in the abundance of SOC functional groups across
 352 vegetation types in different sub lakes (Fig. 7b).

353 Stability indices showed that Mudflat and *Carex* communities had significantly
 354 higher A/O-A ratios, HI indices and aromaticity than *Miscanthus* ($P < 0.05$), while the
 355 Alip/Arom ratio showed the opposite pattern (Fig. 8), suggesting that the mudflat and
 356 *Carex* community formed a more stable organic carbon pool through enrichment of
 357 difficult-to-degrade fractions, such as alkyl C and aromatic C.

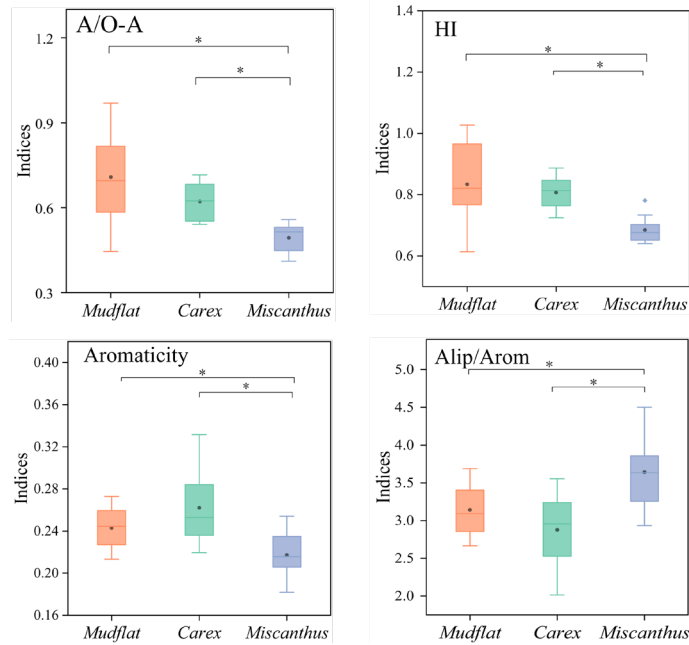
358



359

360 **Figure 7.** SOC functional group abundance in different vegetation types (a) and in
361 different sub lakes (b). EDL: East Dongting Lake; SDL: South Dongting Lake; WDL:
362 West Dongting Lake.

363



364

365 **Figure 8.** SOC stability index for different vegetation types. A/O-A: the ratio of alkyl C
366 over O-alkyl C; HI: hydrophobicity index, the ratio of the sum of alkyl and aromatic C
367 over the sum of O-alkyl and carbonyl C; Alip/Arom, the ratio of the sum of alkyl C and
368 O-alkyl C over aromatic C; AI, aromaticity index, the ratio of aromatic C over the sum
369 of alkyl C, O-alkyl C and aromatic C.

370

371 **4 Discussion**

372 **4.1 SOC content in different vegetation types**

373 Our study showed that the SOC content of mudflat community (6.88 g kg^{-1}) was
374 the lowest, and there was no significant difference in SOC content between the two
375 communities (*Miscanthus*: 13.76 g kg^{-1} and *Carex*: 12.99 g kg^{-1}). These results partially
376 support our first hypothesis that SOC content should be the highest in the *Miscanthus*
377 community, followed by the *Carex* community, with the mudflat exhibiting the lowest
378 SOC content. Although the vegetation biomass of *Miscanthus* community ($2922.9 \pm$
379 300.8 t/km^2) was significantly higher than that of *Carex* community (1391.0 ± 269.7

380 t/km²), the simpler chemical structure of *Miscanthus* SOC (Fig.7) may facilitate its
381 microbial decomposition. The cross-sub-lake comparisons revealed no significant
382 spatial heterogeneity in vegetated SOC content, which was also inconsistent to our first
383 hypothesis. This may be due to the joint influence of vegetation, hydrology and human
384 disturbance on SOC content. The surface SOC content of the Dongting floodplain
385 wetland (11.12 g kg⁻¹) was close to that of the Poyang Lake wetland (9.69 g kg⁻¹) (Yuan
386 et al., 2023), but lower than that of the forested wetland in the middle and lower Elbe
387 River in Germany (33.73 g kg⁻¹) (Heger et al., 2021).

388

389 **4.2 SOC sources in different vegetation types**

390 Our results showed that autochthonous plant were the main source of SOC
391 (*Miscanthus*:53.3±10.6%, *Carex*:52.4%±11.6%, mudflat:47.5±12.5 %) ,which
392 partially supports our second hypothesis that SOC in *Miscanthus* and *Carex* community
393 would primarily originate from autochthonous plant sources; the source of SOC in the
394 mudflat would primarily originate from allochthonous POM. The SOC of *Miscanthus*
395 and *Carex* communities is mainly derived from autochthonous plant which were related
396 to the plant biomass of communities (*Miscanthus*: 2922.9 ± 300.8 t/km², *Carex*:
397 1391.0±269.7 t/km²) (Table 1). Each year autochthonous plants input a large source of
398 carbon into the soil (Zhu et al., 2022). SOC in the mudflat community was also
399 predominantly derived from autochthonous plants, which can be attributed to reduced
400 allochthonous POM inputs. The commissioning of the Three Gorges Dam in 2003, the
401 world's largest hydropower project, fundamentally altered sediment dynamics, reducing
402 downstream sediment transport from 120 × 10⁶ tons/year (pre-dam) to a state of net
403 erosion (2 × 10⁶ tons/year post-dam) (Yu et al., 2018). The reductions in river sediment
404 transport diminished allochthonous POM contributions. Autochthonous plants are also
405 a major source of SOC in Poyang Lake (located in the lower reaches of the Yangtze
406 River), riverine wetlands along Mexico's Pacific coast, and coastal wetlands in the
407 Mississippi River delta (Wang et al., 2016; Kelsall et al., 2023; Adame and Fry, 2016).
408 The source of SOC in Dongting floodplain wetland has a part of the source of plankton

409 (14.3-23.9 %). This is due to the decline in water quality of the lakes and the gradual
410 increase in algae as a result of problems such as the increased intensity of agricultural
411 farming and the use of chemical fertilizers (Ren et al., 2018).

412 POM had the highest SOC contribution to the mudflat community ($35.4 \pm 10.2 \%$), followed by *Carex* ($31.3 \pm 8.3 \%$), and the lowest was *Miscanthus* ($26.8 \pm 8.1 \%$). This may be related to the different elevations of the vegetation communities
413 (*Miscanthus*:>25 m, *Carex*:22-25 m, Mudflat:<22 m) , where higher elevations lead
414 to shorter inundation times, thus limiting particulate organic matter (POM) deposition.
415 In this study, we also found that SDL exhibited the highest POM contribution (32.5 %),
416 followed by WDL (26.3 %), with EDL showing minimal inputs (21.6 %) in *Miscanthus*
417 communities. A parallel pattern emerged with *Carex* communities, where SDL's POM
418 contribution exceeded EDL by 9.1%. This may be due to the following: Firstly, the
419 intensive agricultural activities and urbanization in the Xiangjiang River basins that
420 have increased soil erosion, making more POM enter the SDL (Xiao et al., 2023).
421 Second, the northern part of the SDL receives a large amount of sediment under the top-
422 supporting effect of the outflow of WDL (Zhang et al., 2019). Third, the inundation
423 duration is the longest in the SDL, followed by the WDL, and the EDL has the shortest
424 inundation duration. The extension of inundation duration can improve the deposition
425 of allochthonous POM (Shen et al., 2020). Studies have also shown that the mean mass
426 accumulative rate (MAR) of the SDL is the highest, followed by the WDL, and the EDL
427 is the lowest (Ran et al., 2023). Thus, the spatial heterogeneity of allochthonous POM
428 contributions to SOC across sub-lakes revealed synergistic controls by anthropogenic
429 and hydrodynamic drivers.

432 **4.3 SOC stability in in different vegetation types**

433 Our findings demonstrate that O-alkyl C, primarily derived from carbohydrates,
434 constitutes the dominant fraction (30.5 – 46.8 %) of SOC in Dongting Lake wetlands.
435 This result partially supports our third hypothesis that the structure of SOC in
436 *Miscanthus* and *Carex* should be dominated by O-alkyl C, and the SOC structure of the
437 mudflat should be dominated by aromatic C. The predominance of O-alkyl C across

438 vegetation communities likely reflects the autochthonous origin of SOC from plant-
439 derived inputs. Specifically, the cellulose and hemicellulose components of plant litter
440 decompose rapidly to produce carbohydrates (McKee et al., 2016). O-alkyl C has also
441 been found to be the dominant fraction of SOC in other lakes or river wetland (Yang et
442 al., 2023; Wang et al., 2011)

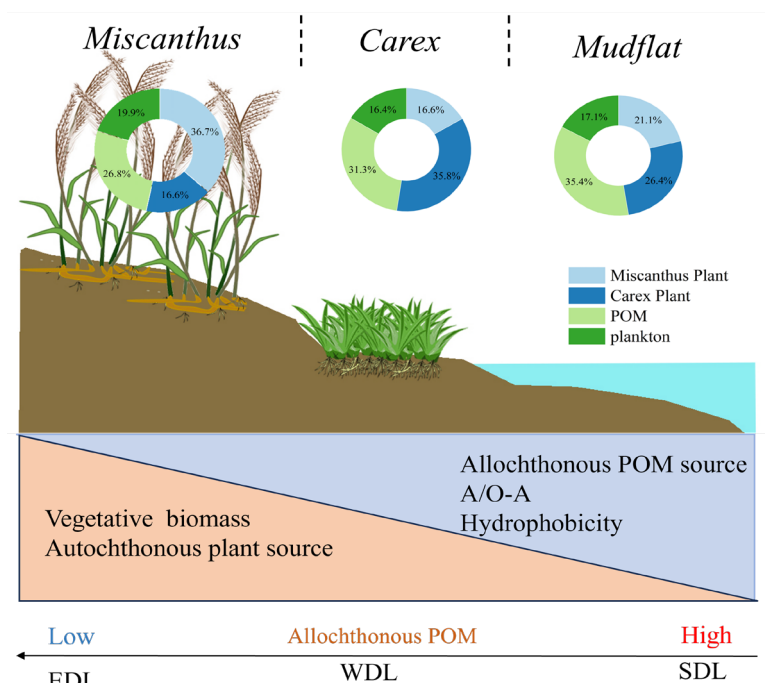
443 Notably, the *Miscanthus* community exhibited significantly higher O-alkyl C
444 content compared to *Carex* and mudflat, while displaying lower alkyl and aromatic C
445 contents (Fig. 7a). Given that O-alkyl C was classified as labile C whereas alkyl and
446 aromatic C were classified as recalcitrant C, these results showed that *Miscanthus*
447 community SOC is more unstable and more susceptible to decomposition. Therefore,
448 the risk of SOC loss is higher in the *Miscanthus* community. The A/O-A and aromaticity
449 as well as HI and Alip/Arom, are recognized as important parameters for evaluating the
450 stability of SOC. The A/O-A ratio, aromaticity and hydrophobicity index (HI) were
451 significantly higher in the *Carex* and mudflat communities than *Miscanthus* community
452 ($P < 0.05$), whereas the Alip/Arom ratio showed the opposite trend, indicating that the
453 SOC of *Carex* and mudflat communities had more complex structures and higher
454 hydrophobicity, which increased SOC stability (Spaccini et al., 2006).

455 O-alkyl C is primarily derived from carbohydrates. *Miscanthus* plants possess a
456 well-developed underground root system that may produce more root secretions,
457 which are mainly composed of carbohydrates (Wu et al., 2021b). The higher aromatic
458 and alkyl C fractions observed in *Carex* and mudflat communities likely result from
459 prolonged inundation duration, which extends exposure to anaerobic conditions.
460 Anoxic conditions significantly limit reactive oxygen species generation and catalase
461 activity, thereby inhibiting oxidative decomposition of lignin (the main component of
462 aromatic carbon) (Benner et al., 1984; Kirk and Farrell, 1987). Additionally, microbial
463 metabolic efficiency declines under oxygen deprivation, retarding the decomposition of
464 lipids and waxes (alkyl carbon precursors) (Keiluweit et al., 2017). These stability
465 difference may be related to the contribution of allochthonous POM. Allochthonous
466 carbon is rich in aromatic and hydrophobic components, exhibiting stronger resistance

467 to decomposition (Keil, 2011). The proportion of allochthonous POM was significantly
468 higher in the *Carex* and mudflat communities than in the *Miscanthus*.

469 The risk of loss of soil carbon pools in *Miscanthus* community is higher due to
470 the more labile molecular structure of SOC (Fig. 9). In our previous research, we also
471 found that the *Miscanthus* community experienced the greatest loss of SOC from 2013
472 to 2022 (Wang et al., 2025). Although the SOC stability of the *Miscanthus* community
473 is relatively low, its SOC content shows no significant difference from that of the *Carex*
474 community due to high litter input (1.258 ± 0.13 Tg C), revealing the differences in the
475 mechanisms of carbon sequestration function formation among different vegetation
476 types in floodplain wetlands (Fig. 9). Therefore, hydrological management strategies
477 such as regulating water levels or extending flood duration could be applied to maintain
478 anaerobic conditions in *Miscanthus* soil, thereby potentially reducing the
479 decomposition rate and loss of SOC. Although this study evaluated SOC stability
480 primarily from the perspective of chemical composition, unaccounted physical and
481 mineral protection mechanisms likely also play significant roles. Therefore, it is
482 necessary to integrate these protective mechanisms into future research considerations.

483



484

485 **Figure 9.** A conceptual map of the sources and stability of SOC on a geomorphic

486 gradient in the Dongting floodplain wetlands. Orange triangles show the decrease in
487 vegetative biomass and autochthonous plant sources from *Miscanthus* (high elevation)
488 to Mudflat (low elevation). In contrast, blue triangles show increases in allochthonous
489 POM sources, A/O-A, and hydrophobicity. The arrows below indicate that from SDL
490 to WDL to EDL, the contribution of allochthonous POM is decreasing. A/O-A: the ratio
491 of alkyl C over O-alkyl C; POM: particulate organic matter; EDL: East Dongting Lake;
492 SDL: South Dongting Lake; WDL: West Dongting Lake.

493

494

495 **5 Conclusions**

496 Stable isotopic analysis demonstrates that SOC in Dongting floodplain wetlands
497 was mainly derived from autochthonous plant inputs, with mean contributions of $53.3 \pm 10.6\%$ (*Miscanthus*), $52.4 \pm 11.6\%$ (*Carex*), and $47.5 \pm 12.5\%$ (mudflat). Notably,
498 allochthonous POM contributions exhibited both vegetation-dependent (mudflat >
499 *Carex* > *Miscanthus*) and regional disparities (SDL>WDL>EDL). We attribute these
500 differences to interacting effects of anthropogenic and hydrodynamic drivers, which
501 collectively regulate allochthonous POM transport and deposition. The A/O-A ratios,
502 aromaticity, and hydrophobicity were lower in *Miscanthus* community, indicating that
503 SOC is more easily decomposed, and the stability of SOC pools is lower. Therefore, we
504 should prioritize the conservation of *Miscanthus* communities SOC to mitigate carbon
505 loss risks.

507

508 **Data availability**

509 The data used in this paper are stored in the open-access online database Figshare (DOI:
510 [10.6084/m9.figshare.30781895](https://doi.org/10.6084/m9.figshare.30781895)).

511

512 **Author contributions**

513 LW: Writing – original draft, Investigation, Data curation. ZD: Writing – review &
514 editing, Project administration, Funding acquisition, Conceptualization. YX: Writing–

515 review & editing, Funding acquisition. TW: Investigation, Data curation. FL: Writing-
516 review & editing, Methodology. YZ: Investigation, Data curation. BW: Formal analysis,
517 Resources. ZH: Methodology, Data curation. CZ: Investigation, Data curation. CP:
518 Writing – review & editing, Formal analysis. AM: Formal analysis, Conceptualization.

519

520 **Competing interests.** The authors declare that they have no conflict of interest.

521

522 **Acknowledgments**

523 This work was supported by the National Key Research and Development Program of
524 China (2023YFF0807202,2022YFC3204101), the National Natural Science
525 Foundation of China (U2444221,U22A20570), the Natural Science Foundation of
526 Hunan Province (2025JJ20039), the Science, Technology and Innovation Platform Plan
527 of Hunan Province, China (2022PT1010).

528

529

530 **Reference**

531 Adame, M. F. and Fry, B.: Source and stability of soil carbon in mangrove and freshwater wetlands of
532 the Mexican Pacific coast, *Wetlands Ecol. Manage.*, 24, 129-137, <http://doi.org/10.1007/s11273-015-9475-6>, 2016.

533 Benner, R., Maccubbin, A. E., and Hodson, R. E.: Anaerobic Biodegradation of the Lignin and
534 Polysaccharide Components of Lignocellulose and Synthetic Lignin by Sediment Microflora, *Appl.*
535 *Environ. Microbiol.*, 47, 998-1004, <http://doi.org/doi:10.1128/aem.47.5.998-1004.1984>, 1984.

536 Boeni, M., Bayer, C., Dieckow, J., Conceiçao, P. C., Dick, D. P., Knicker, H., Salton, J. C., and Macedo,
537 M. C. M.: Organic matter composition in density fractions of Cerrado Ferralsols as revealed by
538 CPMAS ^{13}C NMR: Influence of pastureland, cropland and integrated crop-livestock, *Agric.,*
539 *Ecosyst. Environ.*, 190, 80-86, <http://doi.org/10.1016/j.agee.2013.09.024>, 2014.

540 Boye, K., Noël, V., Tfaily, M. M., Bone, S. E., Williams, K. H., Bargar, J. R., and Fendorf, S.:
541 Thermodynamically controlled preservation of organic carbon in floodplains, *Nat. Geosci.*, 10, 415-
542 419, <http://doi.org/10.1038/ngeo2940>, 2017.

543 Cano, A. F., Mermut, A. R., Ortiz, R., Benke, M. B., and Chatson, B.: ^{13}C CP/MAS-NMR spectra, of
544 organic matter as influenced by vegetation, climate, and soil characteristics in soils from Murcia,
545 Spain, *Can. J. Soil Sci.*, 82, 403-411, 2002.

546 Chen, X., Xu, Y. J., Gao, H. J., Mao, J. D., Chu, W. Y., and Thompson, M. L.: Biochemical stabilization
547 of soil organic matter in straw-amended, anaerobic and aerobic soils, *Sci. Total Environ.*, 625, 1065-
548 1073, <http://doi.org/10.1016/j.scitotenv.2017.12.293>, 2018.

549 Deng, Z. M., Li, Y. Z., Xie, Y. H., Peng, C. H., Chen, X. S., Li, F., Ren, Y. J., Pan, B. H., and Zhang, C.
550 Y.: Hydrologic and Edaphic Controls on Soil Carbon Emission in Dongting Lake Floodplain, China,
551 *Journal of Geophysical Research-Biogeosciences*, 123, 3088-3097,
552 <http://doi.org/10.1029/2018jg004515>, 2018.

553 Doetterl, S., Berhe, A. A., Nadeu, E., Wang, Z. G., Sommer, M., and Fiener, P.: Erosion, deposition and
554 soil carbon: A review of process-level controls, experimental tools and models to address C cycling
555 in dynamic landscapes, *Earth-Sci. Rev.*, 154, 102-122,
556 <http://doi.org/10.1016/j.earscirev.2015.12.005>, 2016.

557 Guo, M., Yang, L., Zhang, L., Shen, F. X., Meadows, M. E., and Zhou, C. H.: Hydrology, vegetation, and
558 soil properties as key drivers of soil organic carbon in coastal wetlands: A high-resolution study,
559 *Environmental Science and Ecotechnology*, 23, <http://doi.org/10.1016/j.ese.2024.100482>, 2025.

560 Heger, A., Becker, J. N., Navas, L. K. V., and Eschenbach, A.: Factors controlling soil organic carbon
561 stocks in hardwood floodplain forests of the lower middle Elbe River, *Geoderma*, 404,
562 <http://doi.org/10.1016/j.geoderma.2021.115389>, 2021.

563 Helfrich, M., Ludwig, B., Buurman, P., and Flessa, H.: Effect of land use on the composition of soil
564 organic matter in density and aggregate fractions as revealed by solid-state ^{13}C NMR spectroscopy,
565 *Geoderma*, 136, 331-341, <http://doi.org/10.1016/j.geoderma.2006.03.048>, 2006.

566 Ji, H., Han, J. G., Xue, J. M., Hatten, J. A., Wang, M. H., Guo, Y. H., and Li, P. P.: Soil organic carbon
567 pool and chemical composition under different types of land use in wetland: Implication for carbon
568 sequestration in wetlands, *Sci. Total Environ.*, 716,
569 <http://doi.org/10.1016/j.scitotenv.2020.136996>, 2020.

570 Gao J, F., Zhang C., Jiang J, H., Huang, Q.: Changes in Sediment Deposition and Erosion and Their
571 Spatial Distribution in the Dongting Lake, *Journal of Geographical Sciences*, 11, 402-410, 2001.

572

573

574 Kayranli, B., Scholz, M., Mustafa, A., and Hedmark, Å.: Carbon Storage and Fluxes within Freshwater
575 Wetlands: a Critical Review, *Wetlands*, 30, 111-124, <http://doi.org/10.1007/s13157-009-0003-4>,
576 2010.

577 Keil, R. G.: Terrestrial influences on carbon burial at sea, *Proc. Natl. Acad. Sci. U. S. A.*, 108, 9729-9730,
578 <http://doi.org/10.1073/pnas.1106928108>, 2011.

579 Keiluweit, M., Wanzek, T., Kleber, M., Nico, P., and Fendorf, S.: Anaerobic microsites have an
580 unaccounted role in soil carbon stabilization, *Nat. Commun.*, 8, <http://doi.org/10.1038/s41467-017-01406-6>, 2017.

582 Kelsall, M., Quirk, T., Wilson, C., and Snedden, G. A.: Sources and chemical stability of soil organic
583 carbon in natural and created coastal marshes of Louisiana, *Sci. Total Environ.*, 867, 12,
584 <http://doi.org/10.1016/j.scitotenv.2023.161415>, 2023.

585 Kendall, C., Silva, S. R., and Kelly, V. J.: Carbon and nitrogen isotopic compositions of particulate
586 organic matter in four large river systems across the United States, *Hydrol. Processes*, 15, 1301-
587 1346, <http://doi.org/10.1002/hyp.216>, 2001.

588 Kirk, T. K. and Farrell, R. L.: ENZYMATIC COMBUSTION - THE MICROBIAL-DEGRADATION
589 OF LIGNIN, *Annu. Rev. Microbiol.*, 41, 465-505,
590 <http://doi.org/10.1146/annurev.mi.41.100187.002341>, 1987.

591 Köchy, M., Hiederer, R., and Freibauer, A.: Global distribution of soil organic carbon – Part 1: Masses
592 and frequency distributions of SOC stocks for the tropics, permafrost regions, wetlands, and the
593 world, *SOIL*, 1, 351-365, <http://doi.org/10.5194/soil-1-351-2015>, 2015.

594 Li, Y., Zhang, H. B., Tu, C., Fu, C. C., Xue, Y., and Luo, Y. M.: Sources and fate of organic carbon and
595 nitrogen from land to ocean: Identified by coupling stable isotopes with C/N ratio, *Estuar. Coast.*
596 *Shelf Sci.*, 181, 114-122, <http://doi.org/10.1016/j.ecss.2016.08.024>, 2016.

597 Liu, S. Y., Li, J. Y., Liang, A. Z., Duan, Y., Chen, H. B., Yu, Z. Y., Fan, R. Q., Liu, H. Y., and Pan, H.:
598 Chemical Composition of Plant Residues Regulates Soil Organic Carbon Turnover in Typical Soils
599 with Contrasting Textures in Northeast China Plain, *Agronomy-Basel*, 12,
600 <http://doi.org/10.3390/agronomy12030747>, 2022.

601 McKee, G. A., Soong, J. L., Caldéron, F., Borch, T., and Cotrufo, M. F.: An integrated spectroscopic and
602 wet chemical approach to investigate grass litter decomposition chemistry, *Biogeochemistry*, 128,
603 107-123, <http://doi.org/10.1007/s10533-016-0197-5>, 2016.

604 Mitsch, W. J., Bernal, B., Nahlik, A. M., Mander, Ü., Zhang, L., Anderson, C. J., Jorgensen, S. E., and
605 Brix, H.: Wetlands, carbon, and climate change, *Landsc. Ecol.*, 28, 583-597,
606 <http://doi.org/10.1007/s10980-012-9758-8>, 2013.

607 Ni, X., Zhao, G. M., White, J. R., Yao, P., Xu, K. H., Sapkota, Y., Liu, J. C., Zheng, H., Su, D. P., He, L.,
608 Liu, Q., Yang, S. X., Yuan, H. M., Ding, X. G., Zhang, Y., and Ye, S. Y.: Source and degradation of
609 soil organic matter in different vegetations along a salinity gradient in the Yellow River Delta
610 wetland, *Catena*, 248, <http://doi.org/10.1016/j.catena.2024.108603>, 2025.

611 Preston, C. M., Newman, R. H., and Rother, P.: USING C-13 CPMAS NMR TO ASSESS EFFECTS OF
612 CULTIVATION ON THE ORGANIC-MATTER OF PARTICLE-SIZE FRACTIONS IN A
613 GRASSLAND SOIL, *Soil Sci.*, 157, 26-35, <http://doi.org/10.1097/00010694-199401000-00005>,
614 1994.

615 Quideau, S. A., Chadwick, O. A., Benesi, A., Graham, R. C., and Anderson, M. A.: A direct link between
616 forest vegetation type and soil organic matter composition, *Geoderma*, 104, 41-60,
617 [http://doi.org/10.1016/s0016-7061\(01\)00055-6](http://doi.org/10.1016/s0016-7061(01)00055-6), 2001.

618 Ran, F W., Nie, X D., Wang, S L., Liao, W F., and Li, Z W.: Evolutionary patterns of the sedimentary
619 environment signified by grain size characteristics in Lake Dongting during the last century, *Journal
620 of Lake Sciences*, 35, 1111-1125, 2023.

621 Ren, J. L., Zheng, Z. B., Li, Y. M., Lv, G. N., Wang, Q., Lyu, H., Huang, C. C., Liu, G., Du, C. G., Mu,
622 M., Lei, S. H., and Bi, S.: Remote observation of water clarity patterns in Three Gorges Reservoir
623 and Dongting Lake of China and their probable linkage to the Three Gorges Dam based on Landsat
624 8 imagery, *Sci. Total Environ.*, 625, 1554-1566, <http://doi.org/10.1016/j.scitotenv.2018.01.036>,
625 2018.

626 Robertson, A. I., Bunn, S. E., Boon, P. I., and Walker, K. F.: Sources, sinks and transformations of organic
627 carbon in Australian floodplain rivers, *Mar. Freshw. Res.*, 50, 813-829,
628 <http://doi.org/10.1071/mf99112>, 1999.

629 Sasmito, S. D., Kuzyakov, Y., Lubis, A. A., Murdiyarso, D., Hutley, L. B., Bachri, S., Friess, D. A.,
630 Martius, C., and Borchard, N.: Organic carbon burial and sources in soils of coastal mudflat and
631 mangrove ecosystems, *Catena*, 187, 11, <http://doi.org/10.1016/j.catena.2019.104414>, 2020.

632 Shen, D. Y., Ye, C. L., Hu, Z. K., Chen, X. Y., Guo, H., Li, J. Y., Du, G. Z., Adl, S., and Liu, M. Q.:
633 Increased chemical stability but decreased physical protection of soil organic carbon in response to
634 nutrient amendment in a Tibetan alpine meadow, *Soil Biol. Biochem.*, 126, 11-21,
635 <http://doi.org/10.1016/j.soilbio.2018.08.008>, 2018.

636 Shen, R. C., Lan, Z. C., Huang, X. Y., Chen, Y. S., Hu, Q. W., Fang, C. M., Jin, B. S., and Chen, J. K.:
637 Soil and plant characteristics during two hydrologically contrasting years at the lakeshore wetland
638 of Poyang Lake, China, *J. Soils Sediments*, 20, 3368-3379, <http://doi.org/10.1007/s11368-020-02638-8>, 2020.

640 Skjemstad, J. O., Clarke, P., Taylor, J. A., Oades, J. M., and Newman, R. H.: THE REMOVAL OF
641 MAGNETIC-MATERIALS FROM SURFACE SOILS - A SOLID-STATE C-13 CP/MAS NMR-
642 STUDY, *Aust. J. Soil Res.*, 32, 1215-1229, <http://doi.org/10.1071/sr9941215>, 1994.

643 Spaccini, R., Mbagwu, J. S. C., Conte, P., and Piccolo, A.: Changes of humic substances characteristics
644 from forested to cultivated soils in Ethiopia, *Geoderma*, 132, 9-19,
645 <http://doi.org/10.1016/j.geoderma.2005.04.015>, 2006.

646 Stock, B. C. and B. X. Semmens. MixSIAR GUI User Manual. Version3.1.
647 <https://github.com/brianstock/MixSIAR/>. doi:10.5281/zenodo.47719, 2016.

648 Swinnen, W., Daniëls, T., Maurer, E., Broothaerts, N., and Verstraeten, G.: Geomorphic controls on
649 floodplain sediment and soil organic carbon storage in a Scottish mountain river, *Earth Surface
650 Processes and Landforms*, 45, 207-223, <https://doi.org/10.1002/esp.4729>, 2020.

651 Wang, F. F., Tao, Y. R., Yang, S. C., and Cao, W. Z.: Warming and flooding have different effects on
652 organic carbon stability in mangrove soils, *J. Soils Sediments*, 10, <http://doi.org/10.1007/s11368-023-03636-2>, 2023.

653 Wang, F. F., Zhang, N., Yang, S. C., Li, Y. S., Yang, L., and Cao, W. Z.: Source and stability of soil organic
654 carbon jointly regulate soil carbon pool, but source alteration is more effective in mangrove
655 ecosystem following *Spartina alterniflora* invasion, *Catena*, 235, 12,
656 <http://doi.org/10.1016/j.catena.2023.107681>, 2024a.

657 Wang, J. J., Dodla, S. K., DeLaune, R. D., Hudnall, W. H., and Cook, R. L.: Soil Carbon Characteristics
658 in Two Mississippi River Deltaic Marshland Profiles, *Wetlands*, 31, 157-166,
659 <http://doi.org/10.1007/s13157-010-0130-y>, 2011.

660 Wang, L. Y., Wang, B. Q., Deng, Z. M., Xie, Y. H., Wang, T., Li, F., Wu, S. A., Hu, C., Li, X., and Hou,

662 Z, Y., Zeng, J., Zou, Y. A., Liu, Z.L., Peng, C, H., Andrew, M.: Surface soil organic carbon losses
663 in Dongting Lake floodplain as evidenced by field observations from 2013 to 2022, *J. Integr. Agric.*,
664 2025.

665 Wang, M. L., Lai, J. P., Hu, K.T., and Zhang, D, L.: Compositions of stable organic carbon and nitrogen
666 isotopes in wetland soil of Poyang Lake and its environmental implications, *China Environmental
667 Science*, 36, 500-505, 2016.

668 Wang, S. L., Ran, F. W., Li, Z. W., Yang, C. R., Xiao, T., Liu, Y. J., and Nie, X. D.: Coupled effects of
669 human activities and river-Lake interactions evolution alter sources and fate of sedimentary organic
670 carbon in a typical river-Lake system, *Water Res.*, 255, 13,
671 <http://doi.org/10.1016/j.watres.2024.121509>, 2024b.

672 Wu, H., Zhang, H. C., Chang, F. Q., Duan, L. Z., Zhang, X. N., Peng, W., Liu, Q., Zhang, Y., and Liu, F.
673 W.: Isotopic constraints on sources of organic matter and environmental change in Lake Yangzong,
674 Southwest China, *Journal of Asian Earth Sciences*, 217, 11,
675 <http://doi.org/10.1016/j.jseas.2021.104845>, 2021a.

676 Wu, J. P., Deng, Q., Hui, D. F., Xiong, X., Zhang, H. L., Zhao, M. D., Wang, X., Hu, M. H., Su, Y. X.,
677 Zhang, H. O., Chu, G. W., and Zhang, D. Q.: Reduced Lignin Decomposition and Enhanced Soil
678 Organic Carbon Stability by Acid Rain: Evidence from ^{13}C Isotope and ^{13}C NMR Analyses, *Forests*,
679 11, 14, <http://doi.org/10.3390/f11111191>, 2020.

680 Wu, Q. Y., Lin, Y. L., Sun, Y. H., Wei, Q. H., Liu, J. T., Li, X. F., and Cui, G. W.: Research Progress on
681 Effects of Root Exudates on Plant Growth and Soil Nutrient Uptake, *Chinese Journal of Grassland*,
682 43, 97-104, 2021b.

683 Xiao, T., Ran, F. W., Li, Z. W., Wang, S. L., Nie, X. D., Liu, Y. J., Yang, C. R., Tan, M., and Feng, S. R.:
684 Sediment organic carbon dynamics response to land use change in diverse watershed anthropogenic
685 activities, *Environ. Int.*, 172, <http://doi.org/10.1016/j.envint.2023.107788>, 2023.

686 Xia, S. P., Wang, W. Q., Song, Z. L., Kuzyakov, Y., Guo, L. D., Van Zwieten, L., Li, Q., Hartley, I. P.,
687 Yang, Y. H., Wang, Y. D., Quine, T. A., Liu, C. Q., and Wang, H. L.: Spartina alterniflora invasion
688 controls organic carbon stocks in coastal marsh and mangrove soils across tropics and subtropics,
689 *Global Change Biology*, 27, 1627-1644, <http://doi.org/10.1111/gcb.15516>, 2021.

690 Xie, Y. H., Yue, T., Chen, X. S., Feng, L., and Deng, Z. M.: The impact of Three Gorges Dam on the
691 downstream eco-hydrological environment and vegetation distribution of East Dongting Lake,
692 *Ecohydrology*, 8, 738-746, <http://doi.org/10.1002/eco.1543>, 2015.

693 Yang, Y., Jia, G. D., Yu, X. X., and Cao, Y. X.: Land use conversion impacts on the stability of soil organic
694 carbon in Qinghai Lake using ^{13}C NMR and C cycle-related enzyme activities, *Land Degrad. Dev.*,
695 34, 3606-3617, <http://doi.org/10.1002/ldr.4706>, 2023.

696 Yu, Y. W., Mei, X. F., Dai, Z. J., Gao, J. J., Li, J. B., Wang, J., and Lou, Y. Y.: Hydromorphological
697 processes of Dongting Lake in China between 1951 and 2014, *J. Hydrol.*, 562, 254-266,
698 <http://doi.org/10.1016/j.jhydrol.2018.05.015>, 2018.

699 Zhang, J. Q., Hao, Q., Li, Q., Zhao, X. W., Fu, X. L., Wang, W. Q., He, D., Li, Y., Zhang, Z. Q., Zhang,
700 X. D., and Song, Z. L.: Source identification of sedimentary organic carbon in coastal wetlands of
701 the western Bohai Sea, *Sci. Total Environ.*, 913, <http://doi.org/10.1016/j.scitotenv.2023.169282>,
702 2024.

703 Zhang, W. L., Gu, J. F., Li, Y., Lin, L., Wang, P. F., Wang, C., Qian, B., Wang, H. L., Niu, L. H., Wang,
704 L. F., Zhang, H. J., Gao, Y., Zhu, M. J., and Fang, S. Q.: New Insights into Sediment Transport in
705 Interconnected River-Lake Systems Through Tracing Microorganisms, *Environ. Sci. Technol.*, 53,

706 4099-4108, <http://doi.org/10.1021/acs.est.8b07334>, 2019.
707 Zhu, L. L., Deng, Z. M., Xie, Y. H., Zhang, C. Y., Chen, X. R., Li, X., Li, F., Chen, X. S., Zou, Y. A., and
708 Wang, W.: Effects of hydrological environment on litter carbon input into the surface soil organic
709 carbon pool in the Dongting Lake floodplain, *Catena*, 208,
710 <http://doi.org/10.1016/j.catena.2021.105761>, 2022.
711